Applied Energy 336 (2023) 120846

Contents lists available at ScienceDirect

Applied Energy

journal homepage: www.elsevier.com/locate/apenergy

Optimal sizing for microgrids integrating distributed flexibility with the Perth West smart city as a case study

Chaimaa Essayeh *, Thomas Morstyn

School of Engineering, University of Edinburgh, EH9 3JL, Edinburgh, UK

GRAPHICAL ABSTRACT

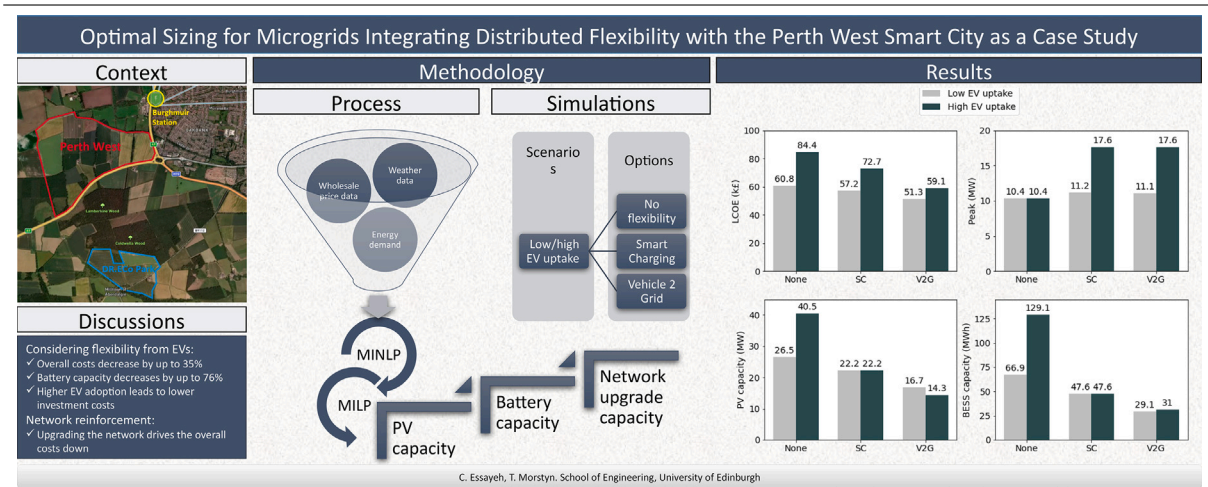

ARTICLE INFO

Keywords:
Optimal sizing
Microgrid
Electric vehicles
Flexible assets
Grid reinforcement
Battery storage system

ABSTRACT

With the decreasing cost of green technologies and the increasing ambitions to reach the net-zero carbon emissions target, more communities are engaged in renewable deployment and energy-intensive technologies such as heat pumps and electric vehicles will be intensively adopted in the near future. The integration of these appliances in lower grid levels will likely require grid reinforcements. However, some of these appliances are flexible and there is an opportunity to explore their flexibility potential to optimise the investment costs further. This paper proposes an optimal design strategy for a grid-connected site that returns the renewable generation and storage's optimal sizing capacities and the required network reinforcement capacity. The novelty of the work is integrating network upgrade costs and considering flexibility from distributed flexible resources across planning and operation. The problem is formulated as a mixed integer piecewise linear problem, with the capacities of generation, storage and network upgrade as decision variables. The piecewise linear cost function related to the upgrade costs figuring in the objective function is then recast as a mixed-integer problem, and the flexible resources are modelled through an approximation method as a single virtual flexible asset. The application of the strategy on the Perth West smart city project as a case study demonstrates the importance of considering flexibility in the planning phase. The costs related to the storage system can decrease by up to 76%, and the overall costs by up to 35%, with the highest levels of savings, reached for the highest rates of electric vehicle adoption.

* Corresponding author.
E-mail address: cessayeh@ed.ac.uk (C. Essayeh).

https://doi.org/10.1016/j.apenergy.2023.120846
Received 19 December 2022; Received in revised form 27 January 2023; Accepted 10 February 2023
Available online 17 February 2023

1. Introduction

The energy sector is the largest responsible for greenhouse emissions with a share of around 75% [1]. Energy-related CO_2 emissions are estimated to increase from 33 GT in 2015 to 35 Gt in 2050 under current and planned policies [2], and if the objectives of the Paris summit agreement are to be met, the share of renewables need to increase from 25% to 85% by 2050 [2]. Thanks to the dropping prices of renewable technologies, reaching almost 80% drop in 10 years [3], increased integration of renewable sources is ongoing. The idea of being less impacted by electricity prices and more energy-independent becomes attractive, and renewable deployment is on a steady rise across utility, commercial, and residential sectors.

To reduce costs using renewables, accurate sizing should be performed during the planning phase to decide on the right capacities of renewable technologies. Different strategies are presented in the literature to minimise the costs of investing in a renewable system. The most popular algorithms are linear programming and their derived models such as mixed integer linear programming (MILP) [4] and robust optimisation (RO) [5], and heuristics algorithms, e.g., particle swarm optimisation (PSO) [6], grey wolf [7], and differential evolution (DE) [8]. Fewer works consider the optimal combination of both generation and storage capacities. The majority of works on storage sizing consider the capacity of the generation (solar panels and/or wind turbines) to be fixed and known in advance [8–10]. The most common objective for the strategies is minimising the investment costs for the renewable system, and fewer papers consider other objectives such as increasing energy autonomy [6] or decreasing CO_2 emissions. For grid-connected sites, no work integrates the network upgrade cost, i.e., installation of new transformers and reinforcement of existing lines, into the objective function.

Although there are studies that analyse the impact of the integration of new technologies such as PV, electric vehicles (EVs) and heat pumps (HPs) on the grid [11–13], and suggest models for the optimised upgrade [11,13], to the best of our knowledge, there is no work that integrates the network costs into the sizing models that perform the sizing for grid-connected sites.

Moreover, one of the constraints that sizing needs to account for is the supply–demand balance, i.e., demand is considered inelastic and has to be met at all times. However, with the emergence of flexible assets and their integration in lower grid levels, there is an opportunity to explore the flexibility to increase energy efficiency and drive the costs even lower when accomplishing the infrastructure investments. Activating flexibility from distributed assets to optimise the operational costs at the distribution level is recurrent in the literature and takes many forms such as solving network congestion [14–16], minimising power loss [17] or addressing voltage deviation [16]. Fewer papers in the literature consider flexibility in the planning phase. Xie et al. [8] considered the flexibility of HPs in the battery sizing model, but network capacity upgrade was not considered. Crozier et al. [18] conducted an analysis of the impact of EV's controlled charging on the required network upgrades. However, the study did not take other flexible resources into account and the optimal renewable system sizing was not considered.

Table 1 summarises the different microgrid optimisation strategies that are found in the literature. They can be structured into three categories: sizing models that optimise the renewable system costs, models that return the optimal network upgrade required to support the integration of new technologies into the grid, and models that optimise the costs during the operation phase by considering flexibility. In the first category, the size of renewable power supply is optimised to serve different purposes such as system cost reductions or CO2 emissions reduction. A detailed overview of the different methods for microgrid sizing can be found in [19,20]. The sizing is a crucial step of the planning phase as it allows decision-makers to have an idea of the investment costs. However, the proposed models in the literature for grid-connected sites do not account for the grid connection point, and the sizing is generally performed under the assumption that the site will keep the same grid connection capacity. This may limit the efficiency of the model as reinforcing the network may reduce the costs. The second category is a part of the planning phase too. An estimation of the required network upgrade that will support the increasing energy demand is conducted, and the estimates are computed under the assumption that the demand will be supplied from the grid connection point. To the best of our knowledge, no work conducts the estimate in the presence of a local renewable system that supplies the site. The third category of strategies studies the potential of some distributed assets in providing flexibility to reduce operational costs or to defer network upgrades. Nevertheless, the potential of these assets was never exploited from a renewable system sizing perspective. Thereby, a strategy that optimises the costs across the three categories is worth investigating.

This paper proposes a sizing model for a grid-connected site that explores flexibility from distributed assets and accounts for the network

Nomenclature

$\eta_b^{ch}, \eta_b^{dis}$	Charging and discharging battery b efficiency
$\eta_{ev}^{ch}, \eta_{ev}^{dis}$	Charging and discharging EV battery ev efficiency
κ^x	The unit price of equipment x
$\mathcal{T}_{avail}$	Availability period of EV ev
$\overline{p}_b^{ch/dis}$	Maximum (dis)charging rate of battery b
$\overline{p}_{ev}^{ch/dis}$	Maximum (dis)charging rate of EV battery ev
$\underline{E}_b, \overline{E}_b$	Minimum and maximum state of charges of battery b
$\underline{E}_{ev}, \overline{E}_{ev}$	Minimum and maximum state of charges of EV battery ev
$\underline{p}_b^{ch/dis}$	Minimum (dis)charging rate of battery b
$\underline{p}_{ev}^{ch/dis}$	Minimum (dis)charging rate of EV battery ev
AF	Annuity Factor
$C_{imp}(t)$	Wholesale energy prices at time step t
E_b^0	The initial state of charge of battery b
$E_{ev}^{arr}, E_{ev}^{arr}$	State of charge at arrival and departure of EV battery ev
$G(t)$	Global horizontal irradiance of the site at time step t
LT	Lifetime
$NOCT$	Nominal operation temperature
$p_b^{ch/dis}(t)$	(Dis)charging power of battery b at time step t
$p_{ev,agg}^{ch/dis}(t)$	Aggregated (Dis)charging power of EV fleet at time step t
$p_{ev}^{ch/dis}(t)$	(Dis)charging power of EV battery ev at time step t
$P_{imp}(t)$	Import power at time step t
P_{peak}	Maximum import power
P_{PV}	Nominal PV panels capacity
$p_{PV}(t)$	Output power of the PV panels at time step t
$P_{PV}^r(t)$	Rated power solar of the site at time step t
r	Discount Factor
$T(t)$	Ambient temperature of the site at time step t
T_{eff}	Temperature coefficient of power

Table 1
Microgrid optimisation strategies proposed in the literature.

Ref	Purpose			Resources			Methods
	Renewable system costs	Network upgrade costs	Operational costs	Generation	Storage	Flexible loads	
[4]	✓			✓	✓		MILP
[6]	✓			✓	✓		PSO
[8]	✓		✓		✓		DE
[9]	✓				✓		MILP
[10]	✓				✓		LP
[11]		✓	✓			✓	LP
[12]		✓	✓	✓	✓	✓	iterative
[13]		✓			✓		MILP
[14]			✓		✓	✓	ADMM
[15]			✓		✓		Bi-level programming
[16]			✓		✓	✓	two-stage stochastic programming
[17]			✓			✓	LP
[18]		✓	✓		✓		LP
[21]	✓			✓	✓		Iterative
[22]			✓		✓	✓	MILP
[23]			✓			✓	LP
[24]			✓	✓	✓	✓	MILP
[25]			✓	✓	✓	✓	iterative price-negotiation
This paper	✓	✓	✓	✓	✓	✓	MILP

upgrade costs. The proposed model is technology-agnostic and integrates flexibility from heterogeneous flexible assets, i.e., thermostatic, deferrable and storage-like assets. Moreover, it integrates the cost of the required network upgrades into the objective function. We apply the proposed model to the Perth West smart city project, which is a greenfield project located in the west of Perth city, UK, and we investigate the impact of considering flexibility during the planning phase on the design decisions of the system, i.e., size of renewable generation, size of the storage system and the required network infrastructure to support the system. The key novelties of the paper can be summarised as follows:

- Unlike existing optimal sizing models that return the optimal capacity sizes of generation and/or storage, we model the optimal sizing of a grid-connected site that considers the costs of network reinforcements and returns, in addition to the optimal generation and storage sizes, the optimal upgrade capacity,
- We integrate the operational flexibility from distributed flexible resources into the proposed sizing model. Taking account of the flexibility of distributed assets during the planning phase can be beneficial and help in deferring infrastructure upgrades and reducing investment costs. The method is scalable and can be applied to heterogeneous sources of flexibility.
- We apply the model to a real-world case study and demonstrate that the co-optimisation of power system investment with the operation of local flexible resources decreases investment costs related to the renewable system.

The rest of the paper is structured as follows. Section 2 formulates the sizing problem as a mixed integer non-linear problem. In Section 3, we present a MILP reformulation of the MINLP model and an approximate aggregation model that reduces the scale of the problem. The resulting formulation is tested on a case study that is presented in Section 4, and Section 5 concludes the paper and opens on future works.

2. Problem formulation

Greenfield microgrid sites present a potential opportunity for the decarbonisation target since their energy system can be designed to maximise the operational value of flexible energy assets. Optimisation across local energy infrastructure and coordination of flexibility will reduce infrastructure costs and unlock new revenue streams for flexible asset owners.

In this section, we present a mathematical formulation for the optimised microgrid investment that integrates the flexibility from distribution resources to return the optimal generation and storage capacities and the optimal grid capacity required to support the connection of the site to the grid.

We consider Perth West smart city project as a case study, therefore, the formulation will focus on solar generation and battery energy storage systems (BESS) as clean energy assets and EVs as flexible resources. We note that the formulation can be straightforwardly extended by including other distributed resources such as wind turbines and/or other sources of flexibility such as thermal and interruptible loads.

2.1. Objective

The optimal sizing problem of a site is initially formulated as a mixed-integer non-linear programming (MINLP) model that aims at minimising the annualised total costs of the system. The total costs include (1) upgrade costs for network infrastructure, (2) capital costs for purchasing, installing and maintaining the equipment, and (3) operational costs of buying electricity from the network. The investment

costs are divided by an annuity factor $AF_{\cdot}$ to reflect the yearly cost, with $AF_{\cdot} = \frac{1-\frac{1}{(1+r)^{LT_{\cdot}}}}{r}$, r refers to the discount factor and $LT_{\cdot}$ to the equipment lifetime. The investment costs for the PV and BESS are assumed to be linear to their nominal capacity, with $\kappa_{\cdot}$ being the unit price of the equipment.

$$\begin{aligned} Cost^{ann}_{total} =& Cost^{ann}_{upg} + Cost^{ann}_{cap} + Cost^{ann}_{op} \\ =& \frac{Cost_{upg}}{AF_{upg}} + \frac{Cost^{PV}_{cap}}{AF_{PV}} + \frac{Cost^{b}_{cap}}{AF_{b}} \\ &+ \sum_{t} C_{imp}(t) P_{imp}(t) \\ =& \frac{f(P_{peak})}{AF_{upg}} + \frac{\kappa^{PV} P_{PV}}{AF_{PV}} + \frac{\kappa^{b} \overline{E}_{b}}{AF_{b}} \\ &+ \sum_{t}^{T} C_{imp}(t) P_{imp}(t) \end{aligned} \tag{1}$$

We consider the upgrade costs to be a piecewise linear function of the peak demand [13]:

$$f(P_{peak}) = a_i P_{peak} + b_i \quad \text{if} \quad P_{peak} \in]u_i, u_{i+1}] \tag{2}$$

Where u_{i+1} is the upper bound of the ith segment of the cost function and u_0 is the lower bound for the interval definition of P_{peak}. b_i is interpreted as the cost of producing and replacing a new transformer to support the required capacity. For example, if we have two transformers T_1 and T_2 supporting capacities up to Cap_1 and Cap_2 respectively then b_i will be assigned the cost of T_2 for P_{peak} in the range of $]Cap_1, Cap_2]$. a_i is the unit cost of reinforcing and expanding existing lines.

The objective function becomes:

$$\begin{aligned} Cost^{ann}_{total} =& \frac{a_i P_{peak} + b_i}{AF_{upg}} + \frac{\kappa^{PV} P_{PV}}{AF_{PV}} + \frac{\kappa^{b} \overline{E}_{b}}{AF_{b}} \\ &+ \sum_{t}^{T} C_{imp}(t) P_{imp}(t), \\ & P_{peak} \in]u_i, u_{i+1}] \end{aligned} \tag{3}$$

We note that the objective function can integrate other costs such as the CO_2 emissions costs [26] and battery degradation costs [27].

2.2. Constraints

The optimisation problem is subject to several constraints that we explain in detail in this subsection.

$$-P_{peak} \leq P_{imp}(t) \leq P_{peak}, \quad \forall t \in \mathcal{T} \tag{4}$$

$$\begin{cases} \underline{p}^{ch/dis}_{b} \leq p^{ch/dis}_{b}(t) \leq \overline{p}^{ch/dis}_{b}, & \text{(a)} \\ \underline{E}_{b} \leq E^{0}_{b} + \sum_{t_0}^{t} (\eta^{ch}_{b} p^{ch}_{b}(\tau) - \frac{p^{dis}_{b}(\tau)}{\eta^{dis}_{b}}).\delta t \leq \overline{E}_{b}, & \text{(b)} \\ \forall t \in \mathcal{T} \end{cases} \tag{5}$$

$$\begin{cases} p_{PV}(t) = P_{PV} P^{r}_{PV}(t) \\ P^{r}_{PV}(t) = \frac{G(t)}{1000} \left[1 - T_{eff} \left(T(t) + \frac{G(t)(NOCT-20)}{800} - 25\right)\right] \end{cases} \tag{6}$$

$$\begin{cases} \underline{p}^{ch/dis}_{ev} \leq p^{ch/dis}_{ev} \leq \overline{p}^{ch/dis}_{ev} & \text{(a)} \\ \underline{E}_{ev} \leq E^{arr}_{ev} + \sum_{t_{arr}}^{t} (\eta^{ch}_{ev} p^{ch}_{ev}(\tau) - \frac{p^{dis}_{ev}(\tau)}{\eta^{dis}_{ev}}).\delta t \leq \overline{E}_{ev}, \forall t \in \mathcal{T}_{avail} & \text{(b)} \\ E^{arr}_{ev} + \sum_{t_{arr}}^{\mathcal{T}_{avail}} (\eta^{ch}_{ev} p^{ch}_{ev}(\tau) - \frac{p^{dis}_{ev}(\tau)}{\eta^{dis}_{ev}}).\delta t = E^{dep}_{ev} & \text{(c)} \end{cases} \tag{7}$$

$$\begin{cases} p^{dis}_{b}(t) - p^{ch}_{b}(t) + \sum_{ev} p^{dis}_{ev}(t) - \sum_{ev} p^{ch}_{ev}(t) \\ + p_{PV}(t) - load(t) + p_{grid} = 0, \quad \forall t \in \mathcal{T} \end{cases} \tag{8}$$

$$P_{PV}, \overline{E}_{b} \in \mathbb{N}^{+} \tag{9}$$

Constraint (4) limits the maximum power that can be exchanged with the grid. The system of equations in (5) defines the operational limits of the battery; Eq. (5)(a) sets the lower and upper limits $\underline{p}^{ch/dis}_{b}$, $\overline{p}^{ch/dis}_{b}$ on the charging/discharging power of the BESS $p^{ch/dis}_{b}$ over the horizon $\mathcal{T}$ of the study, and Eq. (5)(b) limits the capacity of the battery $E_b(t)$ to the range $[\underline{E}_{b}, \overline{E}_{b}]$. The capacity limits of PV generation are expressed in (6). The output of the PV panels is the product of the nominal power of the PV system P_{PV} and the rated solar power of the site P^{r}_{PV}, the latter is computed using different weather information [28], such as the global horizontal radiance of the site G, the temperature of the site T, the temperature coefficient of power T_{eff} and the nominal operation temperature $NOCT$. For each EV, we integrate the operational constraints that are similar to the BESS constraints ((7)(a) and (7)(c)) with one additional constraint requiring the energy in the EV battery at departure E^{dep}_{ev} to be at a certain level (Eq. (7)(b)). We note that the EVs are characterised by an availability period which is expressed through the set $\mathcal{T}_{avail}$. The supply–demand balance is expressed in Eq. (8). The constraint (9) imposes the returned nominal power and capacity to be integers. The optimisation problem is to select the optimal PV nominal power, BESS nominal capacity and grid connection capacity that minimise the annualised total costs:

$$\begin{aligned} \min_{P_{PV}, \overline{E}_{b}, P_{Peak}} \quad & Cost^{ann}_{total} \\ \text{s.t.} \quad & (4) \text{ - } (9) \end{aligned} \tag{10}$$

3. Problem reformulation

The two main limitations of the MINLP formulation are:

- The presence of the non-convex piecewise linear part in the objective function, which is non-solvable by LP solvers;
- The large number of EVs to integrate into the formulation. The number of EV constraints to include are in the order of $\mathcal{T}_d N$ where $\mathcal{T}_d$ is the number of days considered in the set $\mathcal{T}$ and N is the number of EVs. This will result in a resource limitation issue.

In the following subsections, we present a mixed-integer linearisation of the piecewise term of the objective function and an approximate representation of the collection of EVs.

3.1. MILP reformulation of the MINLP model

In the formulation of the problem, the objective function includes a non-linear term $f(P_{peak})$ related to the upgrade costs for the network infrastructure. Though there exist solvers for this type of problem, their resolution becomes intractable and computationally expensive with the increase of the problem size, while MILP presents a good trade-off of computational performance and solution accuracy [29] for large problems. We reformulate the problem as MILP by adopting the method proposed by Trecate et al. [30]. We define three auxiliary variables: δ binary vector variable of size $n-1$ (n being the number of segments in the piecewise function), z real vector variable of size $n-1$ and z_{sum} scalar real variable. The variable z_{sum} will replace the expression $f(P_{peak})$, and the additional mixed-integer linear constraints to be included in the formulation of the problem are presented in (11),

where ϵ is a small tolerance, and m_i and M_i are defined as in (12).

$$\begin{cases}
(u_n-u_0)*\delta_i \le -(u_{i+1}-P_{peak})+(u_n-u_0), & i\in[0,n-1]\\
(u_1-u_n-\epsilon)*\delta_i \le (u_{i+1}-P_{peak})-\epsilon, & i\in[0,n-1]\\
\delta_i-\delta_j\le 0, & i\in[1,n-1], j\in[1,i[\\
(M_1-m_0)*\delta_0-z_0\le -a_1P_{peak}+(M_1-m_0-b_1)\\
(M_0-m_1)*\delta_0+z_0\le a_1P_{peak}+(M_0-m_1+b_1)\\
(m_1-M_0)*\delta_0-z_0\le -a_0P_{peak}-b_0\\
(m_0-M_1)*\delta_0+z_0\le a_0P_{peak}+b_0\\
-M_i\delta_{i-1}+z_{i-1}\le 0, & i\in[2,n-1]\\
m_i\delta_{i-1}-z_{i-1}\le 0, & i\in[2,n-1]\\
-m_i\delta_{i-1}+z_{i-1}\le (a_i-a_{i-1})P_{peak}+(b_i-b_{i-1})-m_i, & i\in[2,n-1]\\
M_i\delta_{i-1}-z_{i-1}\le -(a_i-a_{i-1})P_{peak}+(b_i-b_{i-1})+M_i, & i\in[2,n-1]\\
z_{sum}=\sum_{i=0}^{n-1} z_i
\end{cases} \tag{11}$$

$$\begin{cases}
m_0=a_0u_0+b_0\\
M_0=a_0u_n+b_0\\
m_1=a_1u_0+b_1\\
M_1=a_1u_n+b_1\\
m_i=(a_i-a_{i-1})u_0+(b_i-b_{i-1}), & \forall i\in[2,n]\\
M_i=(a_i-a_{i-1})u_n+(b_i-b_{i-1}), & \forall i\in[2,n]
\end{cases} \tag{12}$$

The system (10) becomes:

$$\begin{aligned}
&\min_{P_{PV},\overline{E}_b,P_{peak},\delta,z} && z_{sum}\\
&\text{s.t.} && (11)
\end{aligned} \tag{13}$$

The MILP approximation of an MINLP model with a piecewise function of n segments will need $2(n-1)+1$ auxiliary variables and $\frac{(n-1)(n+10)}{2}$ additional constraints.

3.2. Approximate aggregation model of DERs

While the consideration of DER flexibility in the planning phase is important as it may lead to significant savings in investment, it can present a challenge in terms of scalability. The number of DERs to be deployed in future sites is estimated to be high and integrating their constraints in the MILP can be computationally burdensome even for the most powerful solvers. In this paper, we adopt the method of approximate aggregation found in [31]. The method starts by modelling the individual assets as polytopes: $P=\{x|Ax\le b\}$, and then gives an outer approximation of their Minkowski sum. The outer approximation may lead to a larger set compared to the exact Minkowski sum. The recovery of a feasible solution from an infeasible solution returned by the outer approximation is presented in the Appendix.

The approximate aggregation can be applied to different flexible assets, e.g., deferrable, thermostatic and storage-like loads. In the case study, we consider the EVs for the flexibility provision. Therefore, in the following, we will focus on EV aggregation modelling. The polytope representation of the constraints associated with an EV is:

$$\begin{bmatrix}
\mathbf{I} & \mathbf{0}\\
-\mathbf{I} & \mathbf{0}\\
\mathbf{0} & \mathbf{I}\\
\mathbf{0} & -\mathbf{I}\\
\eta\Gamma_{tri} & \frac{\Gamma_{tri}}{\eta}\\
-\eta\Gamma_{tri} & -\frac{\Gamma_{tri}}{\eta}
\end{bmatrix}
\begin{bmatrix} p_{ev}^{ch}\\ p_{ev}^{dis}\end{bmatrix}
\le
\begin{bmatrix}
\mathbf{P_{ev}^{max}}\\
\mathbf{0}\\
\mathbf{P_{ev}^{max}}\\
\mathbf{0}\\
\overline{\mathbf{E}}_{\mathbf{ev}}-\mathbf{E}_{\mathbf{ev}}^{\mathbf{0}}\\
\mathbf{E}_{\mathbf{ev}}^{\mathbf{0}}
\end{bmatrix} \tag{14}$$

Where $\mathbf{I}$ and $\mathbf{0}$ are respectively the one and zero vectors of dimension $|\mathcal{T}|$ with $\mathcal{T}$ is the horizon of optimisation, η the efficiency of the EV battery, Γ_{tri} is the lower triangular matrix of shape $|\mathcal{T}|$, $\overline{\mathbf{E}}_{\mathbf{ev}}-\mathbf{E}_{\mathbf{ev}}^{\mathbf{0}}$, $\mathbf{E}_{\mathbf{ev}}^{\mathbf{0}}$ and $\mathbf{P}_{ev}^{\mathbf{max}}$ are vectors of dimension $|\mathcal{T}|$, $\overline{E}_{ev}$ is the maximum capacity of the EV battery and E_{ev}^0 its initial capacity. The values of the vector $\mathbf{P}_{ev}^{\mathbf{max}}$ are defined as follows:

$$P_{ev}^{max}(t)=\begin{cases}\overline{p}_{ev}^{ch}, & \text{if} \quad t\in\mathcal{T}_{avail}\\ 0, & \text{otherwise}\end{cases} \tag{15}$$

where $\mathcal{T}_{avail}$ is the availability period of the EV limited by t_a and t_d which refer respectively to the EV arrival and departure times.

We assume that all EVs have the same efficiency η. Under this assumption, all EVs will share the same A matrix and Eq. (16) will apply. In case the EVs do not share the same A matrix, i.e., they do not have the same efficiency, η, they can be aggregated following the method detailed in [31].

$$P_{agg}=\{z|Az\le\sum_i^N b_i\},\quad z=\sum_i^N x_i \quad \text{and} \quad x_i\in P_i \tag{16}$$

Applying (16) on the EV polytope representation, we derive the list of EV constraints to integrate into the MILP:

$$\begin{bmatrix}
\mathbf{I} & \mathbf{0}\\
-\mathbf{I} & \mathbf{0}\\
\mathbf{0} & \mathbf{I}\\
\mathbf{0} & -\mathbf{I}\\
\eta\Gamma_{tri} & -\frac{\Gamma_{tri}}{\eta}\\
-\eta\Gamma_{tri} & \frac{\Gamma_{tri}}{\eta}
\end{bmatrix}
\begin{bmatrix} p_{ev,agg}^{ch}\\ p_{ev,agg}^{dis}\end{bmatrix}
\le
\begin{bmatrix}
\sum_{\mathbf{i}}^{\mathbf{N}}\mathbf{P}_{\mathbf{ev_i}}^{\mathbf{max}}\\
\mathbf{0}\\
\sum_{\mathbf{i}}^{\mathbf{N}}\mathbf{P}_{\mathbf{ev_i}}^{\mathbf{max}}\\
\mathbf{0}\\
\sum_{\mathbf{i}}^{\mathbf{N}}(\mathbf{E}_{\mathbf{ev_i}}^{\mathbf{max}}-\mathbf{E}_{\mathbf{ev_i}}^{\mathbf{0}})\\
\sum_{\mathbf{i}}^{\mathbf{N}}\mathbf{E}_{\mathbf{ev_i}}^{\mathbf{0}}
\end{bmatrix} \tag{17}$$

where the superscript i refers to the EV's index and N is the total number of EVs. The variables $(p_{ev_i}^{ch})_{i\in[1,N]}$ and $(p_{ev_i}^{dis})_{i\in[1,N]}$ are substituted by the couple variables $p_{ev,agg}^{ch}$ and $p_{ev,agg}^{dis}$, and the number of constraints is reduced from $6N|\mathcal{T}|$ to $6|\mathcal{T}|$.

3.3. Final MILP sizing model

The proposed model for the PV-BESS sizing considering flexibility from home EV charging and network upgrade costs is expressed as follows:

$$\begin{aligned}
&\min_x && Cost_{lin}\\
&\text{s.t.} && \\
& && (5),\ (6),\ (8),\ (9),\ (11),\ (17)
\end{aligned} \tag{18}$$

Where:

$$\begin{aligned}
Cost_{lin}=&\frac{z_{sum}}{AF_{inf}}+\frac{\kappa^{PV}P_{PV}}{AF_{PV}}+\frac{\kappa^b\overline{E}_b}{AF_b}\\
&+\sum_t^T C_{imp}(t)P_{imp}(t)
\end{aligned} \tag{19}$$

and $x=\{P_{PV},\overline{E}_b,P_{peak},\delta,z,p_{ev,agg}^{ch},p_{ev,agg}^{dis},p_b^{ch},p_b^{dis}\}$

4. Case study

Perth West (Fig. 1) is a Greenfield project located in the west of Perth city, UK. Its developers aim to deliver an inclusive, green economic growth agenda. This will include the incorporation of clean technologies to serve smart city growth and support decarbonised

Fig. 1. Perth West, a smart city project located on the western edge of the city of Perth, UK. The project supports 25+ hectares of commercial land and 3500 houses. It will have a network connection to the Burghmuir substation, and will be connected to the DRECO energy park, which is a part of the development and includes solar generation and battery storage.

energy, heat and transport. Lamberkin Villages Urban Innovation is the residential area within the Perth West site which will have 3,500 residential units [32]. In this case study, we investigate the optimal green set-up considering flexibility from EVs for the Lamberkin Villages.

4.1. Settings of the site

Since the site is not developed yet, information on the population, house type and insulation is limited. We base the estimation of the domestic consumption on Profile Class 2 (Domestic Economy 7 Customers) as provided by UKERC Energy Data Centre [33]. The dataset provides the half-hourly electricity consumption of a household under the Economy 7 tariff,[1] for autumn, winter, spring, summer and high summer weekday, Saturday and Sunday. As the site hosts around 3500 residential units, the load profile was up-scaled by a factor of 3500 to approximate the overall electricity consumption from the residential premises of the site (Fig. 2(a)). We note that it is acceptable to directly scale up the energy profile because the method used to extract it includes averaging over a representative sample of customers that captures the diversity within the customer class [33].

Fig. 2(b) shows the solar energy output as a ratio of the nominal capacity of a solar system for the location of Perth based on 2019 weather data [34]. We took T_{eff} (=0.045) and $NOCT$ (=45.5 °C). The overall cost of a utility-scale PV is 770.8 £/kW [3] and includes the hardware, installation expenses and soft costs such as the sales tax and the transmission lines. The overall cost of a utility-scale battery is 162.36 £/kWh [35].

The site will be connected to the distribution network via the Burghmuir substation. The upgrade costs depend predominantly on the installed transformer/substation and the cables/overhead lines that connect the installed transformer(s) to the site. These costs were taken from the DNO proposals. For confidentiality issues, we are not able to publish the upgrade costs in detail. For a capacity lower than 0.76 MW, the site will need no reinforcement and the existing infrastructure can support the site demand. Beyond that capacity, new transformers will need to be installed. The curve of the costs follows a stepwise trend, as presented in Eq. (2), with 8 segments giving costs associated with capacity reinforcements ranging from 0.75 kW to 54.8 kW.

For the wholesale prices, we use historical data for the year 2021 from the EPEX platform as an estimate for future energy prices. Nevertheless, we note that in the future, the prices can have unpredictable

[1] Economy 7 tariff is a time-of-use tariff adopted in the UK with 2 rates (off-peak and peak rates)

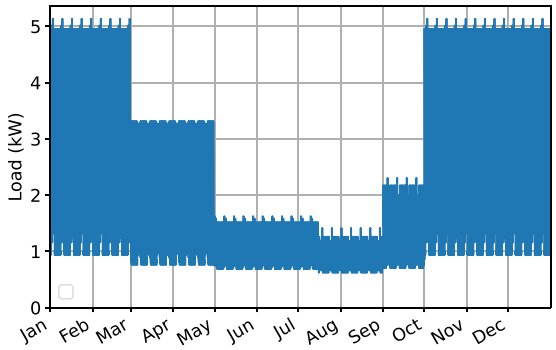

(a) Load profile for a domestic building -Economy 7 Tariff Scheme-

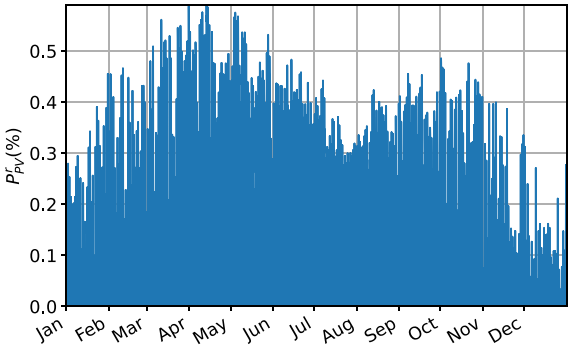

(b) Solar energy rate for the site (2019 data)

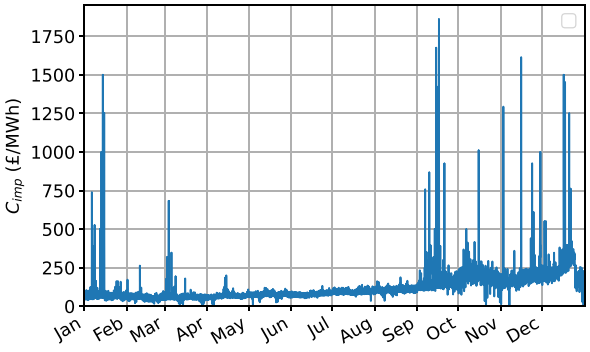

(c) Wholesale energy prices in the UK for the year 2021

Fig. 2. Simulation data.

behaviour due partially to future carbon taxes and mainly due to unstable geo-political circumstances. Fig. 2(c) shows the average half-hourly prices, the mean price is around 117.84 £/MWh with 90% of the prices being less than 200 £/MWh. For residential EV demand, we consider the statistics from the report [36] that estimates ~ 1 vehicle per household in the region combined with the projection study done in [37] that estimates that 17% of cars would be electric by 2032 in the low uptake scenario and 57% in the high uptake scenario. As the site will host 3500 residential units, we included 595 EVs for the low uptake scenario and 1994 EVs for the high uptake scenario. The following additional assumptions are also made:

- All EVs are available at home from 9 pm to 7 am;
- The home charging power rate is 7 kW;
- The level of charge of batteries at arrival ranges between 20% and 60%;

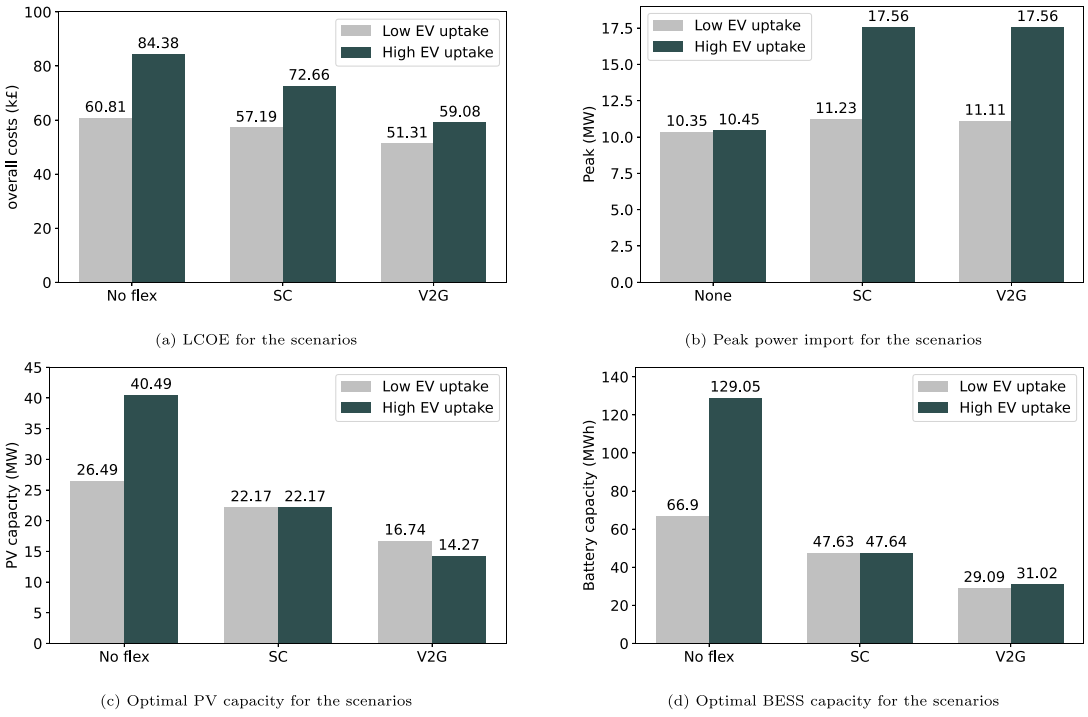

(a) LCOE for the scenarios

(b) Peak power import for the scenarios

(c) Optimal PV capacity for the scenarios

(d) Optimal BESS capacity for the scenarios

Fig. 3. Simulation results for the objective function Fig. 3(a) and the decision variables Figs. 3(b), 3(c) and 3(d).

Table 2
EV parameters.

Parameter	Value
C_{max}	{80, 100} kWh
Depth of discharge	80%
Availability	[8 pm – 7 am]
SOC_{arr}	[0.2–0.4] for C_{max} = 80 [0.4–0.6] for C_{max} = 100
SOC_{dep}	80%
High uptake scenario	56%
Low uptake scenario	17%
Average car per household	1

- The level of charge at departure must be greater than 80%;
- 75% of the EVs have a capacity of 80 kWh and 25% a capacity of 100 kWh.

The lifetime (LT) of the PVs, battery and infrastructure costs are considered to be 25, 10 and 35 years respectively and the discount factor r of the renewable projects is 5%. The simulation data and EV parameters are summurasied in Fig. 2 and Table 2 respectively.

4.2. Results & sensitivity analysis

The results of the strategy are shown in Fig. 3. Fig. 3(a) displays the LCOE for both uptake scenarios under three options: 'No flex' for the business case where no flexibility is activated, SC when the smart charging option is activated and V2G when the vehicle to grid option is activated. The high EV uptake scenario has greater costs compared to the low EV uptake scenario, and for each EV uptake scenario the greatest cost is linked to the 'No flex' option and the lowest cost is reached for the V2G option. However, the decrease is moderate for the low EV uptake scenario (18% decrease between the highest and the lowest cost options) and steep (35%) for the high EV uptake. Those results suggest that the overall costs will increase with the increase of EVs in the network regardless of the selected flexibility scenario. However, the higher the rollout of EVs, the more significant the impact of activating flexibility on the overall costs will be.

In the results of Fig. 3(b), the activation of flexibility (SC or V2G) increases the peak by only 1 MW for the low uptake scenario, while in the case of high EV uptake, the peak import augmented by 7 MW. For both uptake scenarios, the SC and V2G options require more network upgrades compared to the 'No flex' option, this increase is attributable to the SC and V2G strategies aiming at importing more energy from the grid during the off-peak periods to minimise the overall costs. This result shows the importance of considering the network upgrade as part of the objective function. Using conventional sizing strategies, the peak import is set to be fixed to the current network capacity, and this leads to sub-optimal solutions as it limits the exploitation of the full capability of operational flexibility.

Figs. 3(c) and 3(d) show respectively the optimal PV and BESS capacities. From Fig. 3(c), we see a decrease in the optimal PV capacity over the options. In the high uptake scenario, the capacity decreases by 46% and 65.2% for the respective SC and V2G options relatively to the 'No flex' option, the same decrease rates in the low uptake scenarios are 19.2% and 48%. This proves the benefit of activating flexibility. The activation of SC cancels the impact of the EV uptake, i.e., the PV capacity is not impacted by the uptake scenario. The V2G option fully exploits the value of the EVs flexibility, under this option high EV uptake needs less PV capacity compared to the scenario of low EV uptake.

Similarly to the PV optimal capacity, we can see from Fig. 3(d) a decrease in the optimal battery capacity over the different options. In the high uptake scenario, the capacity decreases by 64% and 76% for the respective SC and V2G options relatively to the 'No flex' option, these decrease rates in the low uptake scenarios are 33% and 56.4%. The uptake scenario drastically impacts the battery's size if flexibility is not activated. Almost twice as much battery capacity is needed for the high uptake scenario compared to the low uptake scenario. SC cancels the impact of the EV uptake and both uptake scenarios lead to the same optimal battery capacity in this case. The activation of flexibility will be crucial for higher EV adoption as the required PV and battery

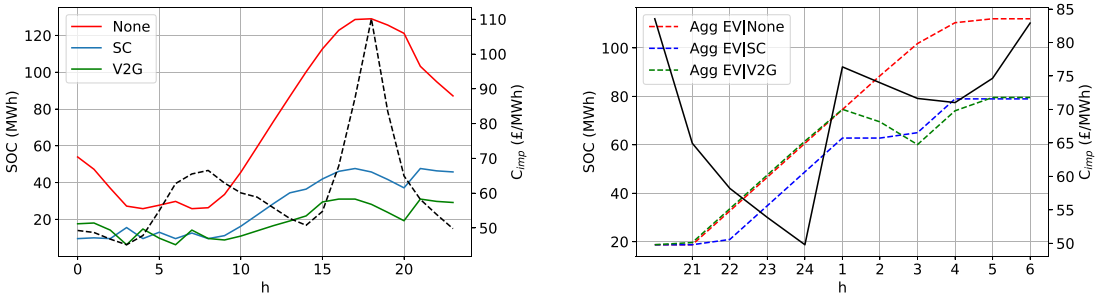

(a) SOC of utility battery for the high uptake scenario

(b) Aggregated SOC of EV fleet for the high uptake scenario

Fig. 4. State of Charge (SOC) of the batteries.

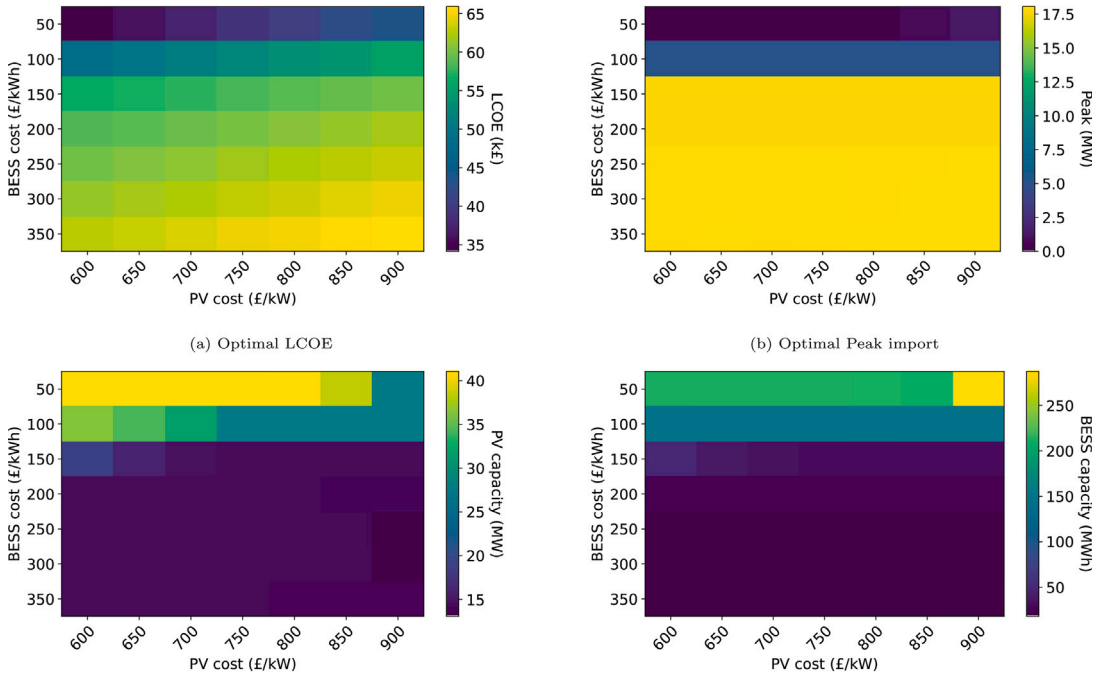

(a) Optimal LCOE

(b) Optimal Peak import

(c) Optimal PV capacity

(d) Optimal BESS capacity

Fig. 5. Impact of PV and battery costs variation on investment costs Fig. 5(a), optimal reinforcement capacity Fig. 5(b), optimal PV capacity Fig. 3(c) and optimal BESS capacity Fig. 5(d).

capacity may become unfeasible to implement (challenge to maintain large batteries and/or secure a large area to implement a large PV capacity).

Fig. 4 shows the SOC behaviour of the utility battery and the aggregated EV battery on a winter day for the high uptake scenario. In Fig. 4(a), we notice that all the options (e.g., no flexibility, SC and V2G) have similar charging patterns: battery keeps charging until prices reach the peak (around 19 h) and then discharge. The difference in battery capacity comes from the fact that the battery in the 'non flex' scenario is larger so that it can discharge to support the charging of EVs when the wholesale prices are higher. The EVs can avoid this in the 'SC' option where they can shift their charging to more economic slots, in Fig. 4(b), the charging stops around 1 am for the SC option when the wholesale price increases and resumes at 2 am when the prices drop. In this same period, we see an EVs' discharge for the V2G scenario, which supports the utility battery discharge to fulfil the load which allows the utility battery capacity to be smaller.

According to [3,35], the projected costs of utility-scale PV and BESS are estimated to be in the ranges of [697, 885] £/kW and [71, 203] £/kWh respectively. We took those intervals as the basis for the sensitivity analysis and we vary the cost of utility-scale PVs and batteries in a range of [600 £/kW - 900 £/kW] and [50 £/kWh - 350 £/kWh] respectively to analyse the impact of technology costs on the decision variables. Fig. 5 shows the results of this analysis. It is noticeable that the PV cost has less impact on the decision variables compared to the battery cost, i.e., for a fixed BESS cost, the peak import, the PV and BESS nominal capacities are almost non-varying across the varying PV cost. This is supported by the results presented in Table 3 that displays the coefficients and the intercept of linear models fitted to link each decision variable to the relation $a_{PV}Cost_{PV} + a_{BESS}Cost_{BESS} + b$. The table shows that the coefficients associated with the PV cost are always less than the coefficients associated with the BESS cost.

In Fig. 5(c), the nominal PV capacity sees a steep decrease of 50% when the BESS cost increases from 100 £/kWh to 150 £/kWh. A lower BESS cost allows the deployment of a higher PV capacity because the excess generation can be profitable if stored using low-cost batteries. The BESS capacity follows a similar pattern as the PV capacity. It sees, as shown in Fig. 5(d), a steep decrease of 70% when the BESS cost increases from 100 £/kWh to 150 £/kWh. The PV cost variation is

Table 3
Fitted linear models.

	PV cost coeff	BESS cost coeff	Intercept
$LCOE$	15.7 kW	72.57 kWh	30.55 £
Peak	0.7 kW^2/£	56.31 kW.kWh/£	167 kW
P_{PV}	−11.75 kW^2/£	−76.71 kW.kWh/£	44.26 kW
$\overline{E}_b$	14.13 kW.kWh/£	−629.22 kWh^2/£	184.49 kWh

shown to have a noticeable impact when the cost of the BESS is 100 £/kWh. In this case, the nominal BESS capacity varies in a range of 1.4 MWh. The peak import varies remarkably for BESS costs in the range [50 £/kWh - 150 £/kWh], beyond this range, the peak stagnates at a value of around 17.5 MW. The high variation of the results for BESS costs in [50 £/kWh - 150 £/kWh] that then stabilise beyond 150 £/kWh is explained by the fact that this range presents the BESS costs that are profitable compared to the price of the utility grid. In this case, the site relies more on generated and stored energy. Beyond 150 £/kWh, it becomes more beneficial for the site to rely more on the energy extracted from the grid. Similarly to the decision variables, the objective function $LCOE$ shows more sensitivity to the BESS cost than to the PV cost. This suggests that the future prices of utility-scale batteries will have a crucial role in the transition to the net-zero target since lower BESS costs imply higher adoption of clean energy, lower costs and minimal grid reinforcement.

5. Conclusion

In this paper, we presented an optimal sizing model that computes the optimal capacities for a grid-connected microgrid and considers, in addition to the renewable system investment costs, the grid connection costs that depend on the peak import. The model accounts for the flexibility of distributed assets in the planning phase and studies its impact on the results. The results demonstrated that the consideration of flexibility can help decrease the renewable system investment costs and that the adoption of renewable systems will rely mainly on the decrease in storage system costs. The costs related to the storage system can decrease by up to 76%, and the overall costs by up to 35%, with the highest levels of savings reached for the highest rates of electric vehicle adoption. Integrating the costs of network reinforcement into the model showed that upgrading the network will be economically beneficial by allowing more energy to be imported in periods of cheaper wholesale prices. In future work, the proposed strategy will be extended to include power flow constraints and improved with a robust version that accounts for the uncertainties from the load and the wholesale prices. Other costs will be considered such as the battery degradation cost, emissions costs and costs for flexibility provision.

CRediT authorship contribution statement

Chaimaa Essayeh: Conceptualization, Methodology, Software, Validation, Formal analysis, Investigation, Data curation, Writing – original draft, Writing – review & editing, Visualization. **Thomas Morstyn:** Conceptualization, Methodology, Writing – review & editing, Supervision, Project administration, Funding acquisition.

Data availability

The upgrade network costs are confidential, the other data is referenced in the references section.

Acknowledgements

The present work has been supported by the EPSRC, United Kingdom grants EP/S031901/1 and EP/(PIV079). The authors thank Perth and Kinross Council and John Dewar Lamberkin Trust for their valuable inputs and insightful remarks.

Appendix. Feasible solution recovery

The formula that recovers a feasible solution **x** from an infeasible approximate solution is as follows:

$$\min_{x_i, i=1,\dots,N} \quad \left\| z - \sum_{i=1}^{N} x_i \right\| \qquad \text{s.t.} \quad A_i x_i \le b_i, \quad i = 1, \dots, N \tag{A.1}$$

where z refers to the outer approximation.

References

[1] Ritchie H, Roser M, Rosado P. Energy. Our World in Data; 2022, https://ourworldindata.org/energy.
[2] Gielen D, Boshell F, Saygin D, Bazilian MD, Wagner N, et al. The role of renewable energy in the global energy transformation. Energy Strategy Rev 2019;24:38–50. http://dx.doi.org/10.1016/j.esr.2019.01.006.
[3] Documenting a decade of cost declines for PV systems. 2021, https://www.nrel.gov/news/program/2021/documenting-a-decade-of-cost-declines-for-pv-systems.html.
[4] Wu D, Ma X, Huang S, Fu T, Balducci P. Stochastic optimal sizing of distributed energy resources for a cost-effective and resilient microgrid. Energy 2020;198:117284. http://dx.doi.org/10.1016/j.energy.2020.117284.
[5] Gong K, Wang X, Jiang C, Shahidehpour M, Liu X, et al. Security-constrained optimal sizing and siting of BESS in hybrid AC/DC microgrid considering post-contingency corrective rescheduling. IEEE Trans Sustain Energy 2021;12(4):2110–22. http://dx.doi.org/10.1109/TSTE.2021.3080707.
[6] Bandyopadhyay S, Mouli GRC, Qin Z, Elizondo LR, Bauer P. Techno-economical model based optimal sizing of PV-battery systems for microgrids. IEEE Trans Sustain Energy 2020;11(3):1657–68. http://dx.doi.org/10.1109/TSTE.2019.2936129.
[7] El-Bidairi KS, Nguyen HD, Mahmoud TS, Jayasinghe S, Guerrero JM. Optimal sizing of battery energy storage systems for dynamic frequency control in an Islanded microgrid: A case study of flinders Island, Australia. Energy 2020;195:117059. http://dx.doi.org/10.1016/j.energy.2020.117059.
[8] Xie C, Wang D, Lai CS, Wu R, Wu X, et al. Optimal sizing of battery energy storage system in smart microgrid considering virtual energy storage system and high photovoltaic penetration. J Clean Prod 2021;281:125308. http://dx.doi.org/10.1016/j.jclepro.2020.125308.
[9] Amini M, Khorsandi A, Vahidi B, Hosseinian SH, Malakmahmoudi A. Optimal sizing of battery energy storage in a microgrid considering capacity degradation and replacement year. Electr Power Syst Res 2021;195:107170. http://dx.doi.org/10.1016/j.epsr.2021.107170.
[10] Salman UT, Al-Ismail FS, Khalid M. Optimal sizing of battery energy storage for grid-connected and isolated wind-penetrated microgrid. IEEE Access 2020;8:91129–38. http://dx.doi.org/10.1109/ACCESS.2020.2992654.
[11] Brinkel N, Schram W, AlSkaif T, Lampropoulos I, van Sark W. Should we reinforce the grid? Cost and emission optimization of electric vehicle charging under different transformer limits. Appl Energy 2020;276:115285. http://dx.doi.org/10.1016/j.apenergy.2020.115285.
[12] Gupta R, Pena-Bello A, Streicher KN, Roduner C, Farhat Y, Thöni D, et al. Spatial analysis of distribution grid capacity and costs to enable massive deployment of PV, electric mobility and electric heating. Appl Energy 2021;287:116504. http://dx.doi.org/10.1016/j.apenergy.2021.116504.
[13] Cui Q, Weng Y, Tan C-W. Electric vehicle charging station placement method for urban areas. IEEE Trans Smart Grid 2019;10(6):6552–65. http://dx.doi.org/10.1109/TSG.2019.2907262.
[14] Shen F, Wu Q, Jin X, Zhou B, Li C, et al. ADMM-based market clearing and optimal flexibility bidding of distribution-level flexibility market for day-ahead congestion management of distribution networks. Int J Electr Power Energy Syst 2020;123:106266. http://dx.doi.org/10.1016/j.ijepes.2020.106266.
[15] Steriotis K, Šepetanc K, Smpoukis K, Efthymiopoulos N, Makris P, et al. Stacked revenues maximization of distributed battery storage units via emerging flexibility markets. IEEE Trans Sustain Energy 2022;13(1):464–78. http://dx.doi.org/10.1109/TSTE.2021.3117313.
[16] Kara G, Pisciella P, Tomasgard A, Farahmand H, Crespo del Granado P. Stochastic local flexibility market design, bidding, and dispatch for distribution grid operations. Energy 2022;253:123989. http://dx.doi.org/10.1016/j.energy.2022.123989.

[17] Gazafroudi AS, Khorasany M, Razzaghi R, Laaksonen H, Shafie-khah M. Hierarchical approach for coordinating energy and flexibility trading in local energy markets. Appl Energy 2021;302:117575. http://dx.doi.org/10.1016/j.apenergy.2021.117575.

[18] Crozier C, Morstyn T, McCulloch M. The opportunity for smart charging to mitigate the impact of electric vehicles on transmission and distribution systems. Appl Energy 2020;268:114973. http://dx.doi.org/10.1016/j.apenergy.2020.114973.

[19] Kiehbadroudinezhad M, Merabet A, Abo-Khalil AG, Salameh T, Ghenai C. Intelligent and optimized microgrids for future supply power from renewable energy resources: A review. Energies 2022;15(9). http://dx.doi.org/10.3390/en15093359.

[20] Hannan M, Faisal M, Jern Ker P, Begum R, Dong Z, et al. Review of optimal methods and algorithms for sizing energy storage systems to achieve decarbonization in microgrid applications. Renew Sustain Energy Rev 2020;131:110022. http://dx.doi.org/10.1016/j.rser.2020.110022.

[21] Essayeh C, El-Fenni M, Dahmouni H. Optimal sizing of a PV-ESS microgrid system under dynamic pricing of utility energy. 2018, p. 86–91. http://dx.doi.org/10.1109/MELCON.2018.8379073.

[22] Zhang Y, Campana PE, Yang Y, Stridh B, Lundblad A, et al. Energy flexibility from the consumer: Integrating local electricity and heat supplies in a building. Appl Energy 2018;223:430–42. http://dx.doi.org/10.1016/j.apenergy.2018.04.041.

[23] Jiang T, Li Z, Jin X, Chen H, Li X, et al. Flexible operation of active distribution network using integrated smart buildings with heating, ventilation and air-conditioning systems. Appl Energy 2018;226:181–96. http://dx.doi.org/10.1016/j.apenergy.2018.05.091.

[24] Olivella-Rosell P, Bullich-Massagué E, Aragüés-Peñalba M, Sumper A, Ottesen Sd, et al. Optimization problem for meeting distribution system operator requests in local flexibility markets with distributed energy resources. Appl Energy 2018;210:881–95. http://dx.doi.org/10.1016/j.apenergy.2017.08.136.

[25] Morstyn T, Teytelboym A, McCulloch MD. Designing decentralized markets for distribution system flexibility. IEEE Trans Power Syst 2019;34(3):2128–39. http://dx.doi.org/10.1109/TPWRS.2018.2886244.

[26] Cao B, Dong W, Lv Z, Gu Y, Singh S, et al. Hybrid microgrid many-objective sizing optimization with fuzzy decision. IEEE Trans Fuzzy Syst 2020;28(11):2702–10. http://dx.doi.org/10.1109/TFUZZ.2020.3026140.

[27] Morstyn T, Teytelboym A, Hepburn C, McCulloch MD. Integrating P2P energy trading with probabilistic distribution locational marginal pricing. IEEE Trans Smart Grid 2020;11(4):3095–106. http://dx.doi.org/10.1109/TSG.2019.2963238.

[28] Essayeh C, Raiss El-Fenni M, Dahmouni H, Ahajjam MA. Energy management startegies for smart green microgrid systems: A systematic literature review. J Electr Comput Eng 2021. http://dx.doi.org/10.1155/2021/6675975.

[29] Moretti L, Manzolini G, Martelli E. MILP and MINLP models for the optimal scheduling of multi-energy systems accounting for delivery temperature of units, topology and non-isothermal mixing. Appl Therm Eng 2021;184:116161. http://dx.doi.org/10.1016/j.applthermaleng.2020.116161.

[30] Trecate GF, Letizia P, Spedicato M. Optimization with piecewise-affine cost functions. Technical report, Zurich, Switzerland: Swiss Federal Institute of Technology (ETH); 2001.

[31] Barot S, Josh A T. A concise, approximate representation of a collection of loads described by polytopes. Int J Electr Power Energy Syst 2017;84:55–63. http://dx.doi.org/10.1016/j.ijepes.2016.05.001.

[32] Perth west. 2022, https://www.perthwest.com/.

[33] Electricity user load profiles by profile class. 2017, https://data.ukedc.rl.ac.uk/browse/edc/efficiency/residential.

[34] https://www.renewables.ninja/ [Accessed: June 2022].

[35] Cost projections for utility-scale battery storage: 2021 update. 2021, https://www.nrel.gov/docs/fy21osti/79236.pdf [Accessed: June 2022].

[36] High granularity projections for low carbon technology uptake - electric vehicle, heat pumps and solar PV. Technical report, Regen; 2020.

[37] Distribution future electricity scenarios in the north of Scotland: Distributed generation and demand technology growth to 2032. Technical report, Regen; 2019.

Update

Applied Energy

Volume 355, Issue , 1 February 2024, Page

DOI: https://doi.org/10.1016/j.apenergy.2023.122257

Applied Energy 355 (2024) 122257

Contents lists available at ScienceDirect

Applied Energy

journal homepage: www.elsevier.com/locate/apenergy

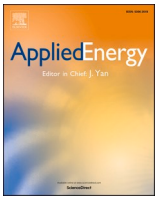

Corrigendum to "Optimal sizing for microgrids integrating distributed flexibility with the Perth West smart city as a case study" [APEN 336, 2023 [120846]]

Chaimaa Essayeh *, Thomas Morstyn

School of Engineering, University of Edinburgh, EH9 3JL Edinburgh, UK

The authors regret to inform the readers that there was an error in describing the results. Where it should be '**annualised total costs**', it is written LCOE. This error figures in:

1. Top-left figure of the results in the graphical abstract,
2. Caption of Figure 3.a,
3. First sentence of subsection 4.2,
4. Last paragraph of subsection 4.2 (in math mode),
5. Figure 5.a: caption and y-axis,
6. Table 3: the first column of the first row,
7. Table 3: 30.55 £ should be £30.55k last column first row.

The authors would like to apologise for any inconvenience caused.

DOI of original article: https://doi.org/10.1016/j.apenergy.2023.120846.
* Corresponding author.
E-mail address: cessayeh@ed.ac.uk (C. Essayeh).

https://doi.org/10.1016/j.apenergy.2023.122257

Available online 7 November 2023